SENSITIVY ANALYSIS OF A PRESSURIZED SOLAR VOLUMETRIC RECEIVER: HEAT TRANSFER FLUIDS AND PRESSURE RATIO COMPARISON

Judit García-Ferrero[1]*, Rosa Pilar Merchán[2], María Jesús Santos[3], Alejandro Medina[4], Antonio Calvo Hernández[5]

Universidad de Salamanca, Department of Applied Physics and Institute of Fundamental Physics and Mathematics (IUFFyM), Salamanca, Spain

[1]jgferrero@usal.es, [2]rpmerchan@usal.es, [3]mjesus@usal.es, [4]amd385@usal.es, [5]anca@usal.es

*Corresponding Author

ABSTRACT

Concentrated Solar Power (CSP) is a promising option within the renewable energy scenario. In recent years, CSP scope is broadening from electricity production to thermal energy applications, including water desalination or solar fuel production, which requires temperatures between 700 to 1500 ºC, which can be achieved through highly concentrated solar flux. Parabolic dish collectors (PDC) are related to the greatest concentration factor within CSP systems that leads to temperatures close to 1000 ºC at the solar receiver. Those solar receivers, in charge of turning solar energy into thermal energy, are the most critical components within CSP systems regarding associated losses. In this work, the performance of a pressurized solar volumetric receiver integrated into a PDC is simulated. Heat transfers are modelled together with the main thermal losses, aiming to describe the system as realistic as possible. The solar receiver model, which has already been validated in previous works, includes detailed geometrical parameters and material properties. Six fluids (dry air, N_2, CO_2, He, Ar and Ne) are analysed as possible heat transfer fluids in the receiver. The thermodynamic properties of those different heat transfer fluids are computed as temperature and pressure dependent employing the NIST-Mathematica database. The thermal efficiency of the solar receiver is strongly affected by the type of heat transfer fluid selected while the receiver inlet pressure slightly affects the performance. For the same mass flow rate, the gas with the higher isobaric heat capacity leads to higher thermal efficiency but also to a reduced average temperature inside the solar receiver. For this solar receiver configuration, helium presents the largest thermodynamic potential to achieve high solar receiver thermal efficiencies (0.854 at 290 K ambient temperature, 400 K inlet temperature, 507 kPa inlet pressure and 0.0881 kg/s mass flow rate), while argon the lowest. This analysis is expected to pave the way for multi-objective studies in order to design solar volumetric receivers and select the best performance heat transfer fluid.

1 INTRODUCTION

Solar energy, particularly Concentrated Solar Power (CSP) systems, stands as one of the most promising renewable energy technologies within the energy transition framework due to both the high efficiencies that can be reached and the possibility to store thermal energy (Merchán et al., 2022). Parabolic dish collectors (PDC) are the most efficient CSP systems due to their largest concentration factor [1000-3000] when compared with other collectors such as parabolic troughs or linear Fresnel collectors [60-80], or solar towers [300-1000] (Belgasim et al., 2018; International Renewable Energy Agency, 2023). These systems can be used for small scale generation, for instance for distributed applications, in order to produce power or heat at small scale ([0.01-0.4] MW) close to the consumption site. Energy production in remote areas is another interesting market where parabolic dishes could be competitive. Nevertheless, PDC can also be grouped in so-called parabolic dishes arrays or farms to produce power or heat on a larger scale. Traditionally, parabolic dishes have been devoted to electric energy production

https://doi.org/10.52202/077185-0020

by means of a thermodynamic cycle, either Stirling (Schiel & Keck, 2012) or, more recently, Joule-Brayton (micro-gas turbines) (Giostri & Macchi, 2016; Lanchi et al., 2015; Semprini et al., 2016). However, within the last years, the focus of CSP systems has gradually widen from electricity to thermal energy generation. Specifically, some innovative applications where PDCs play an important role due to the high temperature requirements includes water treatment, such as water desalination (David Sánchez Martínez et al., 2019) or distillation, or solar fuel production, including hydrogen (Boretti, 2023; Escamilla et al., 2022).

Besides, Thermal Energy Storage (TES) options, which are already implemented effectively in larger CSP installations (Merchán et al., 2022), are starting to be considered for PDC. The most common configuration considered to integrate TES into PDC implies the use of Phase Change Materials (PCM), *i.e.* solid-to-liquid or liquid-to-gas phase change materials that harness the latent heat for storing energy (Sathish et al., 2023; Senthil, 2021). Those PCMs are generally designed to be placed at the PDC solar receiver, allowing for short period (15-20 min) of TES, rectifying solar irradiance fluctuations.

Solar receivers, which turn the solar irradiance into thermal energy, are the most critical components of a CSP system, not only in which TES refers, but especially in high-temperature applications. This energy conversion process involves many heat transfers and radiation exchanges which need to be carefully analysed to establish an accurate performance prediction. The challenging issues for improving the solar receiver performance are focused, among others, on geometry, for minimizing heat losses, and materials, which eventually must withstand increasingly larger temperatures (Gavagnin, 2018; Ho & Iverson, 2014).

Additionally, the type of Heat Transfer Fluid (HTF) employed within the solar receiver influences the solar-to-thermal efficiency. Bellos *et al.* (Bellos et al., 2016, 2017) studied different working fluids in a parabolic trough CSP configuration, aiming to determine the optimum operating conditions of each of them. They focused on air, nitrogen, carbon dioxide, helium, argon, and neon evaluating the influence of the mass flow rate and the inlet temperature to predict which combination leads to the highest exergy efficiency (Bellos et al., 2016). First, they found out that helium reported the best performance, probably due to its greater heat transfer coefficient, and that it operates with the lowest mass flow rate. Carbon dioxide was the most suitable working fluid at high temperature levels (greater than 700 K) while neon and argon reported the lowest performance for all the temperature levels considered. Regarding nitrogen and air, both showed similar efficiency results. Air has some advantages, such as been abundance and being harmless, which can counterbalance its medium performance (Bellos et al., 2016).

Nevertheless, to the authors' knowledge, no comprehensive thermodynamic study exists in literature about the effect of different HTFs on a pressurized solar volumetric receiver of a PDC system, which is the main goal of this paper. Therefore, in this work a pressurized solar volumetric receiver model previously developed by the same research group (García Ferrero, 2023) has been enhanced to test the influence of different HTFs apart from the already analysed one (air). The selection of the five additional HTFs (nitrogen, carbon dioxide, helium, argon, and neon) has been supported on (Bellos et al., 2016) study and other literature works. Moreover, another objective of the work is to assess the effect of some key variables on receiver thermal performance.

2 RECEIVER MODEL

The model developed in this work considers an axially cylindrical pressurized volumetric receiver as it is seen in Figure 1. After the development of the model, the design proposed by Zhu *et al.* (Zhu et al., 2020) has been considered for validation and numerical applications. Nevertheless, the geometry can be modified or scaled in a straightforward manner to be adapted to other CSP systems, such as Central Solar Towers. This type of solar receiver has been considered for high-temperature applications, as water desalination or solar fuel production, since they can reach temperatures above 1000ºC and efficiencies larger than 80% (García Ferrero et al., 2023). The model developed in (García Ferrero et al., 2023), which is the basis for this work, includes novel features barely touched in previous publications: more accurate expressions for thermal radiation exchanges, different temperatures inside and outside the glass window and a volumetric (instead of superficial) heat transfer coefficient for describing the heat exchange within the porous absorbing medium. That model is adapted in this work to study the performance of the solar receiver under new boundary conditions and situations that have

https://doi.org/10.52202/077185-0020

not been previously analysed: different pressure and temperature intervals and different working fluids and mass flow rates. Thus, those are the main novel contributions of this paper.

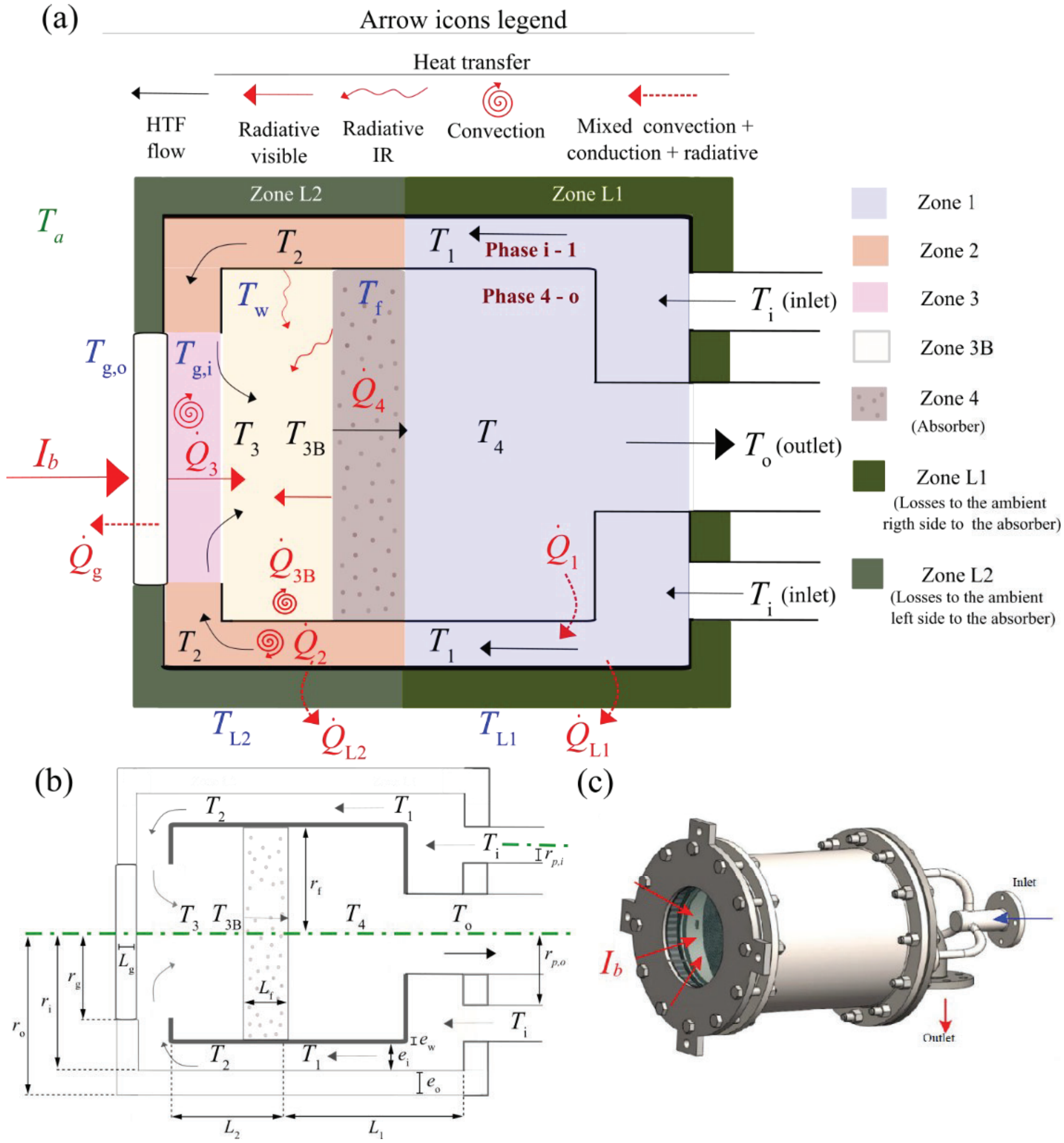

Figure 1: (a) Scheme of the receiver modelled for this work (Zhu et al., 2020). Heat Transfer Fluid (HTF) temperatures (T_i, T_1, T_2, T_3, T_{3B}, T_4 and T_o) are depicted in black. Surfaces temperatures related to glass (inner and outer surfaces), internal wall, absorber foam, front external insulator, and back external insulator ($T_{g,i}$, $T_{g,o}$, T_w, T_f , T_{L1} and T_{L2}, respectively) in blue and ambient temperature (T_a) is depicted in green. Thermal power exchanges ($\dot{Q}_1$, $\dot{Q}_2$, $\dot{Q}_3$, $\dot{Q}_{3B}$, $\dot{Q}_4$, $\dot{Q}_{L1}$, $\dot{Q}_{L2}$ and I_b) are depicted in red. (b) Geometrical parameters used in the heat transfer model of the receiver. (c) 3D image of the receiver (taken from Zhu *et al.* (Zhu et al., 2020)).

Pressurized volumetric receivers are usually built with a ceramic foam or a metal rack in the core, with a large thermal capacity and characterized with a given porosity. This porous element will provide the largest amount of thermal energy to the Heat Transfer Fluid (HTF), thus boosting the solar-to-thermal receiver efficiency. A brief explanation about the heat transfers occurring inside different zones of the receiver is provided next.

https://doi.org/10.52202/077185-0020

Zone 1. It can be split in two phases: phase i-1 (from the receiver inlet until the end of Zone 1), and phase 4-o (from Zone 1 after the absorbing foam until the receiver outlet). The colder air (at temperature T_i) receives heat ($\dot{Q}_1$) from the HTF going out of the receiver that has a higher temperature (T_o). Thus, the air arrives at Zone 2 at temperature T_1. Due to this heat exchange, the temperature at the receiver exit, T_o, is slightly lower than the air temperature just after crossing the absorber foam (T_4). The heat transfer can be modelled as a mixed convection and conduction process (similar to the heat transfer within a heat exchanger, which has been assumed to be perfect, without losses), through the following equations:

$$\dot{Q}_1 = \dot{m}\, \bar{c}_p(T_1,T_i)\,(T_1 - T_i) + \dot{Q}_{L1} = \dot{m}\, \bar{c}_p(T_4,T_o)(T_4 - T_o) \tag{1}$$

$$\dot{Q}_1 = \mathrm{U}\,\mathrm{A}_1 \frac{(T_o\text{-}T_i) - (T_4\text{-}T_1)}{\log\dfrac{(T_o - T_i)}{(T_4 - T_1)}} \tag{2}$$

The most relevant parameters involved in those expressions, apart from the temperatures, are the mass flow ($\dot{m}$), the geometrical parameters (included in A_1 that represents the effective Zone 1 area), and the global convection and conduction heat transfer coefficient (U), which has been calculated as the inverse of the total thermal resistance, through the computation of the Nusselt number for flat plates within phase i -1 and phase 4-o (see (García Ferrero et al., 2023). Finally, $\bar{c}_p(T_h,T_c)$ stands for the isobaric heat capacity average value, obtained by means of a definite integral between the highest (T_h) and the lowest (T_c) temperatures.

Zone 2. There is a heat transfer ($\dot{Q}_2$) through the inner cylinder wall (at temperature T_w) to the HTF, which raises its temperature from T_1 to T_2. $\dot{Q}_2$ comes from the thermal and visible radiation emitted by the absorber foam and the glass window to the inner cylinder wall. The equations describing this heat transfer are analogous to Eqs. (1) and (2). The only difference is that, here, only convection is considered. Thus, parameter U is replaced by h_{wo}, a convection heat transfer coefficient (see (García Ferrero et al., 2023) for explicit definitions). Besides, an energy balance equation should be considered:

$$\dot{Q}_2 = \tau_g I_b F_{gf}\, \rho_f\, F_{fw} + \tau_g I_b F_{gw}\left(1\text{-}\ \rho_w F_{wf} - \rho_w F_{wg}\right) + \frac{\sigma\left(T_f^4\text{-}T_w^4\right)}{\frac{1\text{-}\varepsilon_f}{A_f\varepsilon_f} + \frac{1}{A_f F_{fw}} + \frac{1\text{-}\varepsilon_w}{A_w\varepsilon_w}} - \frac{\sigma\left(T_w^4\text{-}T_{g,i}^4\right)}{\frac{1\text{-}\varepsilon_w}{A_w\varepsilon_w} + \frac{1}{A_w F_{wg}} + \frac{1\text{-}\varepsilon_g}{A_g\varepsilon_g}} - \dot{Q}_{3B} \tag{3}$$

The key parameters within Eq. (3) are the view factors (F_{ij}), transmissivity, reflectivity and emissivity (τ, ρ and ε, respectively) of the materials involved within the heat transfer, and Stefan-Boltzmann constant (σ) for radiative law.

Zone 3. The air receives a heat flux $\dot{Q}_3$ by means of convection with the inner glass surface (at temperature $T_{g,i}$). Thus, the HTF achieves temperature T_3. Additionally, the heat balance at the glass window must be considered, following an equation like Eq. (3). Within Zone 3, the glass absorptivity (α_g) and a natural convection coefficient, h_{go}, are introduced. This last parameter considers the Nusselt number over a flat plate with a characteristic diameter equal to the root-squared glass window aperture area.

Zone 3B. The air exchanges heat flux, $\dot{Q}_{3B}$, through convection with the inner wall surface (at temperature T_w). Hence, the HTF arrives at the absorber foam at temperature T_{3B}. $\dot{Q}_{3B}$ influences the energy balance at Zone 2. The equations governing the heat transfer here are analogous to Eqs. (1) and (2) but including a different convection coefficient (h_{wi}) and a different effective area denoted by A_w.

https://doi.org/10.52202/077185-0020

Zone 4. The fluid crosses the absorber foam (at temperature T_f), receiving thus a heat flux $\dot{Q}_4$. In this stage, the air rises its temperature up to T_4. The heat transfer corresponds to a convection with the pores inside the absorber foam. Although the equations describing this phenomenon are similar to Eqs. (1) and (2), the convection inside the pores is described by a volumetric convective heat transfer coefficient (h_{vf}). That volumetric coefficient will depend on different geometrical parameters that characterize the foam, such as porosity (ϕ), pores diameter (d_p), and superficial foam area (A_f). The Nusselt number employed here to obtain the convective heat transfer coefficient is taken from (Wu et al., 2011), and it has a strong dependence on porosity. Moreover, an energy balance equation, similar to Eq. (3) is also needed to describe the heat transfer within this zone.

Zones L1 and L2 (heat losses at the insulator). The heat transfer across the insulator surfaces will be modelled as a heat transfer within a heat exchanger by means of equations analogous to (1) and (2). The last heat exchange occurring at the outer insulator surface presents a different form of combining convection and radiation processes within the same equation:

$$\dot{Q}_{\mathrm{L}} = \mathrm{A_o}\left(\mathrm{h_{c,L}} + \mathrm{h_{r,L}}\right)(T_{\mathrm{L}} - T_a) \tag{4}$$

where A_o represents the insulator outer surface area and T_L denotes the insulator temperature (zone L1 or L2). $h_{c,L}$ is the convective coefficient and $h_{r,L}$ stands for the radiation coefficient that can be written as follows (Kalogirou, 2014)

$$\mathrm{h_{r,L}} = \varepsilon_{\mathrm{L}}\sigma\,(T_{\mathrm{L}} + T_a)\left(T_{\mathrm{L}}^2 + T_a^2\right) \tag{5}$$

where ε_L is the outer insulator surface emissivity.

Further details about all the equations, parameters considered, and assumptions of this heat transfer model can be checked at (García Ferrero et al., 2023).

2.1 Receiver thermal energy efficiency

The receiver thermal efficiency, η_{rec}, is defined as the ratio between the heat absorbed by the receiver and the total heat flux impinging at the receiver aperture area:

$$\eta_{\mathrm{rec}} = \frac{\dot{Q}_{\mathrm{rec}}}{\mathrm{I_b}} = \frac{\dot{\mathrm{m}}\left(\bar{\mathrm{h}}_{\mathrm{o}} - \bar{\mathrm{h}}_{\mathrm{i}}\right)}{\eta_{\mathrm{opt}}\,\mathrm{A_d}\,\mathrm{DNI}} \tag{6}$$

where $\dot{Q}_{rec}$ stands for the heat flux absorbed by the fluid at the receiver. It can be calculated in terms of the fluid mass flow through the receiver, $\dot{m}$, and the difference between the outlet and inlet fluid-specific enthalpies, $\bar{h}_o$ and, respectively. I_b is the solar radiation power impinging at the solar receiver window. This parameter can be expressed as the product of the parabolic dish optical efficiency, η_{opt}, the dish aperture area, A_d, and the Direct Normal Irradiance (DNI).
The receiver thermal efficiency, η_{rec}, can also be expressed as a function of heat losses as follows:

$$\eta_{\mathrm{rec}} = 1 - \frac{\dot{Q}_g + \dot{Q}_{L1} + \dot{Q}_{L2} + \rho_g I_b}{\mathrm{I_b}} \tag{7}$$

where the term $\rho_g I_b$ accounts for the share of solar energy radiation reflected by the glass window, and $\dot{Q}_g$, $\dot{Q}_{L1}$ and $\dot{Q}_{L2}$ represent the heat losses across the glass window and the insulator L1 and L2 zones, respectively.

https://doi.org/10.52202/077185-0020

2.2 Model validation

The solar receiver validation has been performed by comparing the receiver thermal efficiency outputs with those provided by Zhu *et al.* (Zhu et al., 2020). The relative difference obtained for the thermal efficiency is below 1.5% for all the cases, as shown in Figure 2. Although a greater deviation is observed at the interval ends, those deviations do not overcome the 1.5% mentioned. More details about the validation process can be found in (García Ferrero et al., 2023).

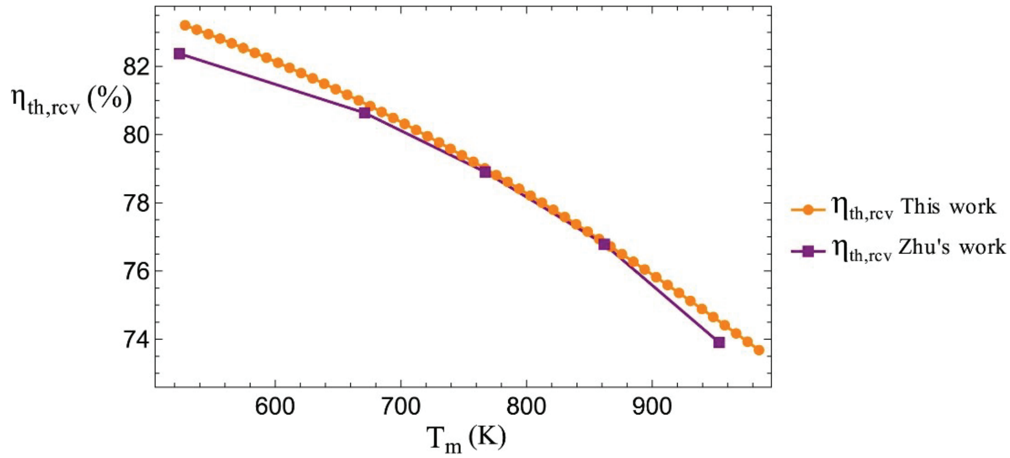

Figure 2: Solar receiver thermal efficiency as a function of mean receiver temperature, T_m: comparison between Zhu's model (Zhu et al., 2020) (purple) and this work (orange).

3 MODEL IMPLEMENTATION

The receiver model has been implemented in Mathematica® programming language. The aperture area of the parabolic dish is 113.10 m^2 and its optical efficiency, 0.8830 (Giostri & Macchi, 2016). Considering that receiver glass window area is 0.0491 m^2, a concentration factor of 2304 is achieved, in accordance with literature (Belgasim et al., 2018). This glass window has a transmissivity at visible wave of 0.851. Regarding the absorbing foam inside the receiver, its radius and its width are 0.182 m and 0.065 m, respectively. Moreover, the emissivity of this foam reaches 0.95. Further details of the geometrical and heat transfer parameters can be found at (García Ferrero et al., 2023).

Following (Bellos et al., 2016) approach, six working fluids have been selected as HTFs for the solar receiver. Table 1 gathers these six fluids together with their molar masses. Other fluid properties are obtained by employing NIST Standard Reference Database 23 (Lemmon et al., 2013), which is directly linked to Mathematica® software. When not indicated specifically, a fluid mass flow rate of 0.0881 kg/s is considered.

The system has been analysed at on-design conditions with a direct normal irradiance of 1000 W/m^2.

Table 1: Molar mass of the six Heat Transfer Fluids considered.

Heat Transfer Fluid	Air	N_2	CO_2	He	Ar	Ne
Molar mass (g/mol)	28.960	28.014	44.009	4.0026	39.948	20.180

4 RESULTS & DISCUSSION

The main objective of this work is to analyse how the ambient temperature, the receiver inlet temperature and the receiver inlet pressure influence the receiver thermal efficiency when six different fluids are considered as Heat Transfer Fluids. For that, a first 3D plot is devoted to the performance of the most traditional fluid (air) as a function of the three aforementioned variables (see Figure 3). Ambient temperature is varied in a noteworthy smaller interval than inlet temperature and inlet pressure due to ambient constraints. On the other hand, both inlet temperature and pressure ranges are much

https://doi.org/10.52202/077185-0020

wider since compressors with different characteristics could be coupled with this solar receiver, the inlet pressure range could be translated into a pressure ratio interval in which compressors could operate. Specifically, since inlet pressure is varied between 304.0 kPa and 608.0 kPa, the corresponding pressure ratio interval could be 3-6 for atmospheric pressure as inlet pressure. The pressure boundary conditions have been selected considering the usual pressure ratio that micro-gas turbines report, since those are the usual power blocks coupled to this system (Giostri & Macchi, 2016; Semprini et al., 2016) . The highest values of the receiver thermal efficiency are associated with high ambient temperatures and both low receiver inlet pressures and temperatures. It can be observed that larger variations on receiver efficiency are expected when changing the inlet temperature comparing with ambient temperature due to the wider considered inlet temperatures range. Nevertheless, not even the wide range of inlet pressures can make the receiver efficiency to be varied in a significant amount.

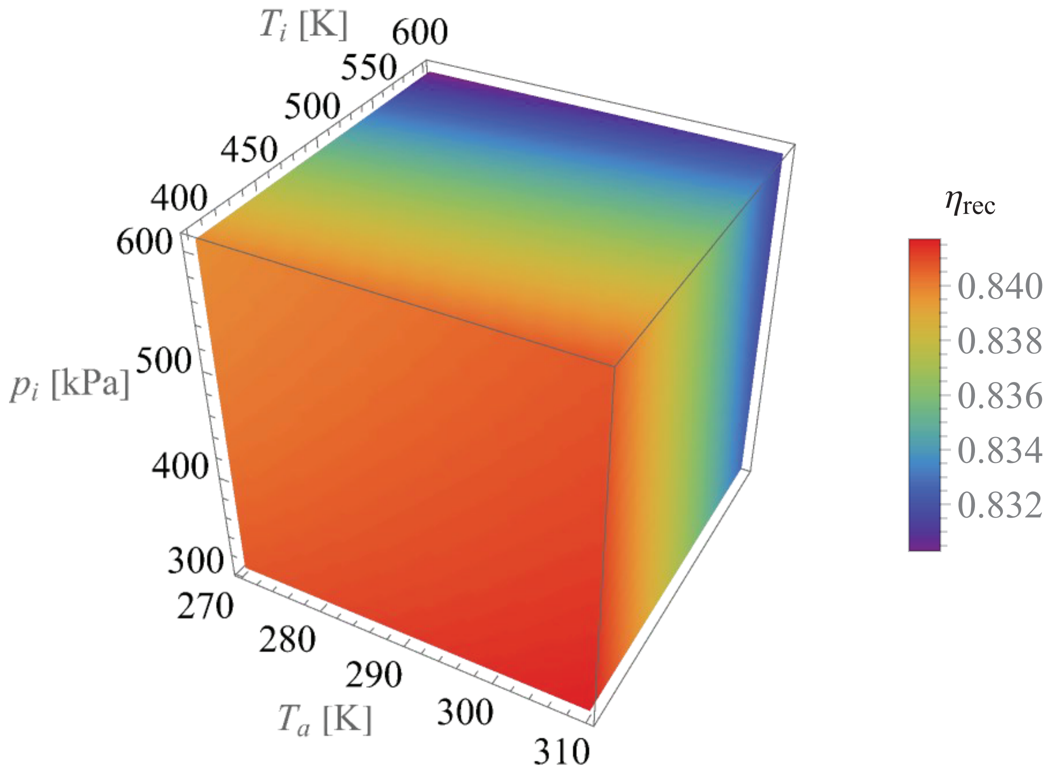

Figure 3: Receiver thermal efficiency (η_{rec}) as a function of ambient temperature (T_a), receiver inlet temperature (T_i) and pressure (p_i) for air with a flow mass rate of 0.0881 kg/s.

The sole effect of each of the three variables is studied alone by performing cross-sections in Figure 3. In this way, Figure 4-Figure 6 (one for each variable) are obtained for the six fluids. An inlet temperature of 500 K and an inlet pressure of 507 kPa (which would correspond to a pressure ratio of 5 for a HTF entering a compressor at atmospheric pressure) are selected when varying the ambient temperature at Figure 4. The receiver increases its thermal efficiency with the ambient temperature because of the associated decrease in system radiation, convection and conduction losses. Helium presents the highest efficiency in the whole ambient temperature range, being able to reach an efficiency of 0.851, and argon, the lowest (0.807). Performance of carbon dioxide, nitrogen and air is really similar. Neon efficiency is around 0.26% lower than air.

Figure 5 shows the effect of receiver inlet temperature when ambient temperature is 290 K and inlet pressure, 507 kPa. The higher the HTF inlet temperature, the less potential for the receiver to increase this HTF temperature, given that the direct normal irradiance is fixed, and so the solar radiation power impinging at the receiver window, I_b (see Eqs. (6) and (7)). Hence, a rise in the inlet temperature leads

https://doi.org/10.52202/077185-0020

to a decrement in the receiver thermal efficiency. In the 200 K width (400 K – 600 K) considered inlet temperature range, receiver efficiency is reduced by 1.27% as maximum, which occurs for neon case. Fluids performance with respect to themselves is similar to ambient temperature case (see Figure 4). The only significant difference is that the higher the inlet temperature, the larger the difference between neon and air/N_2/CO_2, that is to say, the four curves tend to diverge. Maximum efficiency of 0.854 is reached by helium at 400 K inlet temperature.

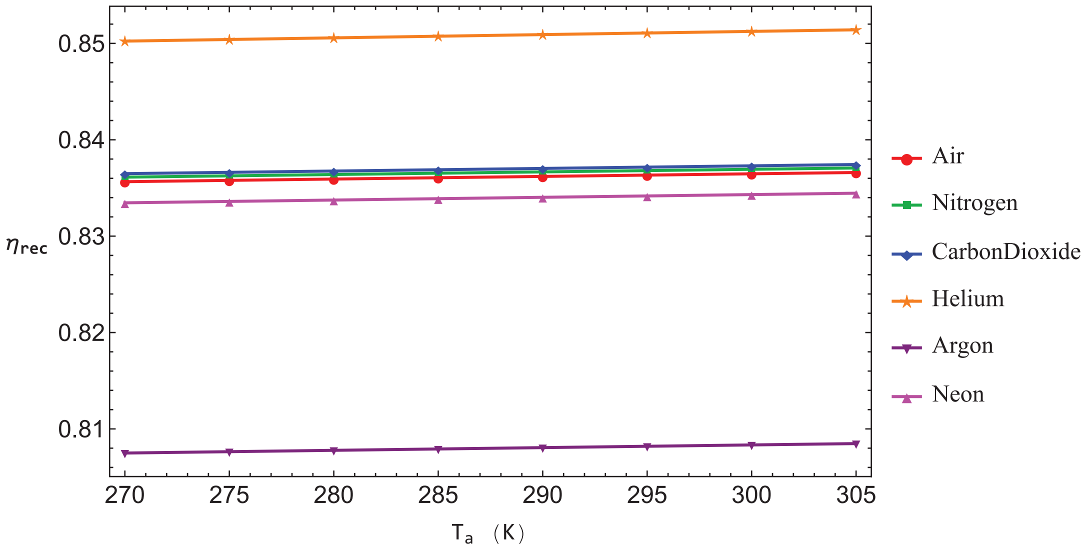

Figure 4: Receiver thermal efficiency (η_{rec}) as a function of ambient temperature (T_a) for the six analysed fluids with a flow mass rate of 0.0881 kg/s, an inlet temperature of 500 K and an inlet pressure of 507 kPa.

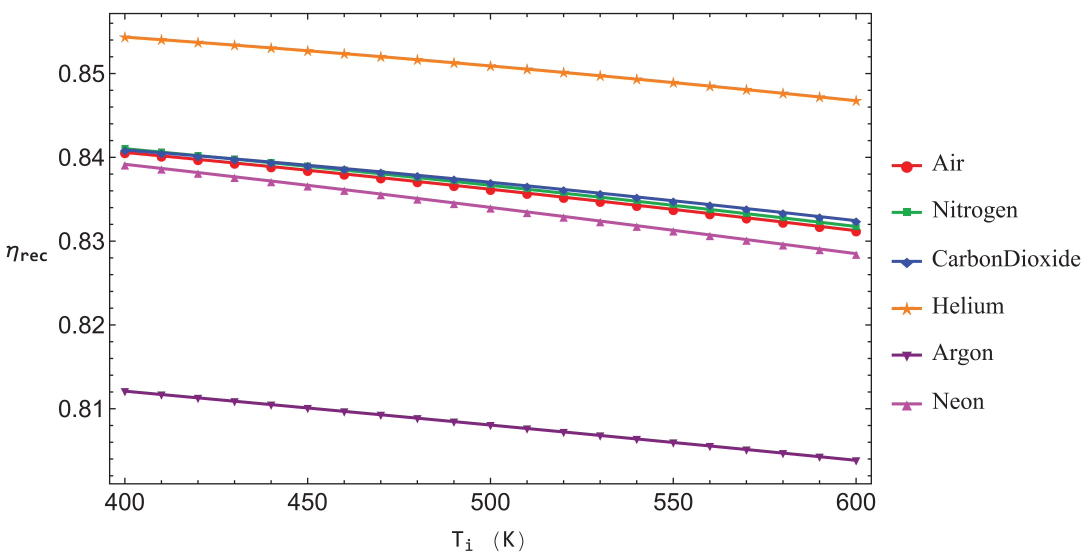

Figure 5: Receiver thermal efficiency (η_{rec}) as a function of receiver inlet temperature (T_i) for the six analysed fluids with a flow mass rate of 0.0881 kg/s, an ambient temperature of 290 K and an inlet pressure of 507 kPa.

https://doi.org/10.52202/077185-0020

Receiver inlet pressure has little effect on receiver thermal efficiency, as it can be observed at Figure 6: a large growth of inlet pressure reduces slightly receiver efficiency. The same fluids performance as before is found.

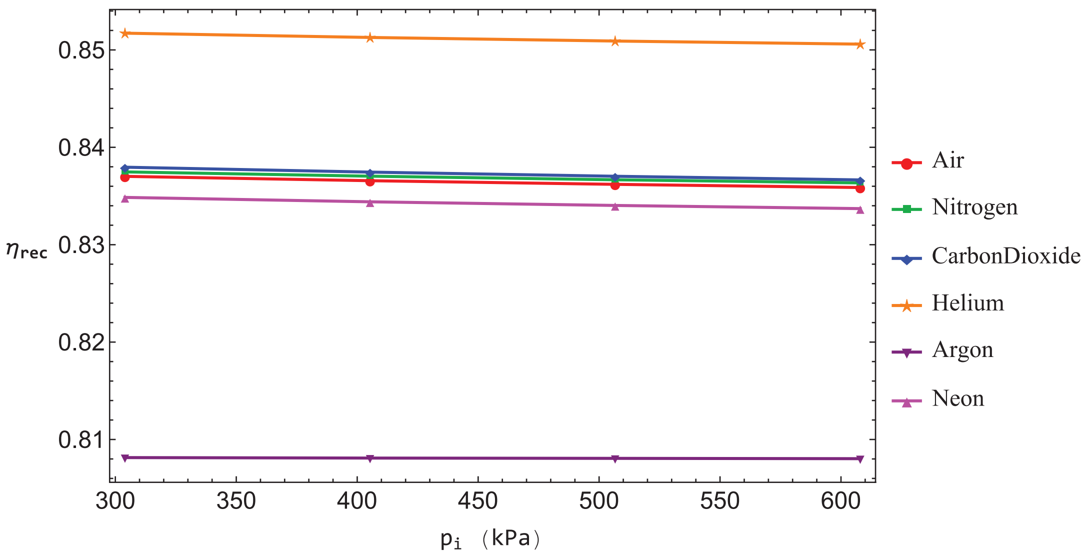

Figure 6: Receiver thermal efficiency (η_{rec}) as a function of receiver inlet pressure (p_i) for the six analysed fluids with a flow mass rate of 0.0881 kg/s, an ambient temperature of 290 K and an inlet temperature of 500 K.

Apart from the previous ambient temperature, inlet temperature and inlet pressure analyses, another goal of this study is to evaluate the receiver performance under different mass flow rates, which is displayed at Figure 7. Mass flow is varied in the interval [0.03-0.15] kg/s, which translates in a thermal power range of [79.2-84.4] kW_{th}. This thermal power is in accordance with (Giostri & Macchi, 2016) study. An interesting behaviour is found: receiver efficiency increases with mass flow, but not linearly and at diverse rates for each fluid. The higher the mass flow, more thermal power can be transmitted, and so, the more efficient the receiver (see Eq. (6)). Helium keeps as the most efficient fluid; however, the difference with the rest of the fluids is decreased substantially for large values of the mass flow. In this way, reducing the inlet temperature (Figure 5) is more effective for rising receiver efficiency than increasing mass flow in the case of helium (the opposite occurs for the rest of the HTFs). Overall, all fluids efficiencies tend to get closer as the mass flow is increased. This means that differences on molar mass among HTFs become negligible in the limit of really large mass flow rates because of the large number of moles involved. Argon remains also as the HTF associated with the lowest receiver efficiency. Nevertheless, it could take values in a wide range [0.770-0.830]. CO_2, N_2, air and Ne present intermediate receiver efficiencies, but their curves cut each other. Thus, for really small mass flows, neon performs better than the other three values. However, when low-medium mass flows are considered, carbon dioxide is more efficient. On the other hand, for cases with large mass flow, CO_2, N_2, air and Ne behave equally. An important outcome of this study is that, when small mass flows are selected, noble gases like helium and neon are preferred, but for large mass flows, the HTFs selection is not so crucial.

In general, other values of the fixed variables do not modify results substantially, and the same qualitative outputs and trends are achieved.

5 CONCLUSIONS

A previously developed model for a solar receiver of a Parabolic Dish Collector has been upgraded for simulating the performance of six Heat Transfer Fluids. The influence of ambient temperature, receiver

https://doi.org/10.52202/077185-0020

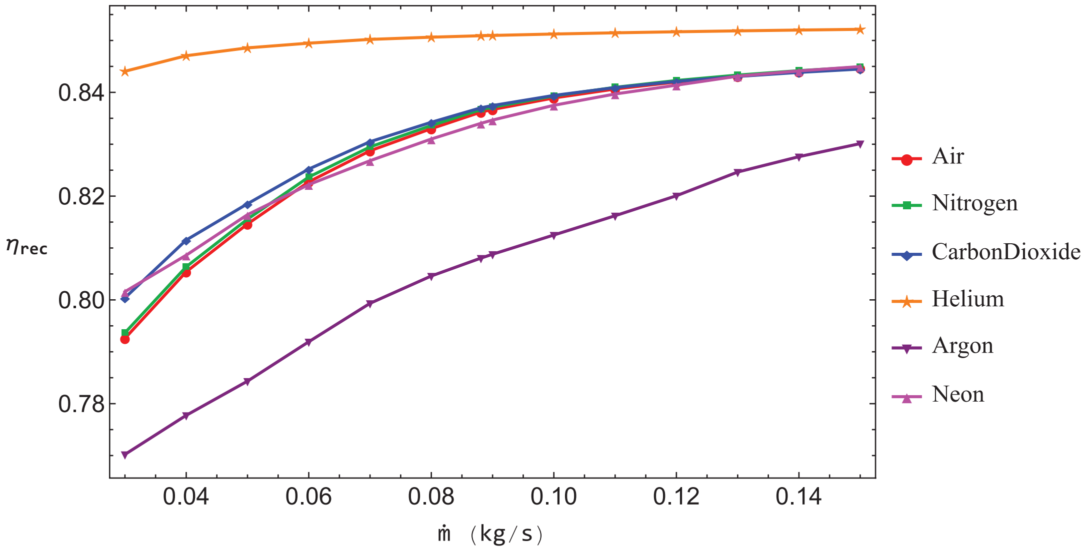

Figure 7: Receiver thermal efficiency (η_{rec}) as a function of mass flow rate ($\dot{m}$) for the six analysed fluids with an ambient temperature of 290 K, an inlet temperature of 500 K and an inlet pressure of 507 kPa.

inlet temperature, receiver inlet pressure and mass flow rate on receiver thermal efficiency has been studied. Both high ambient and low receiver inlet temperatures improve receiver efficiency. On the other hand, inlet pressure effect on receiver performance is almost null. As a general outcome, helium has been found as the HTF able to lead to the highest receiver thermal efficiency compared with the other five fluids considered (air, N_2, CO_2, Ar and Ne). Among analysed variables, mass flow rate has been demonstrated to be the one with the highest potential to enhance receiver efficiency. For small mass flows, noble gases as He and Ne are preferred, but for large ones, fluid selection is not so decisive. Air, N_2 and CO_2 lead always to similar results; thus, among them, air is recommended due to simplicity. Moreover, argon has been totally discarded as an option due to its low performance.
Finally, it could be stated that the Heat Transfer Fluid election for the solar receiver PDC should be based on mass flow rate looking at the thermodynamics point of view. Nevertheless, next step of this work is to analyse HTFs behaviour techno-economically since other variables could affect HTF choice when standing up at economic viewpoint.

NOMENCLATURE

Acronyms

CSP	Concentrated Solar Power	
DNI	Direct Normal Irradiance	
HTF	Heat Transfer Fluid	
PDC	Parabolic Dish Collector	
TES	Thermal Energy Storage	
Regular symbols		
$\dot{m}$	mass flow rate	(kg/s)
p	pressure	(Pa)
$\dot{Q}$	heat rate or thermal power	(W)
T	temperatures	(K)
η	efficiency	(-)
Subscripts		
a	ambient	
i	receiver inlet	
o	receiver outlet	
rec	receiver	

https://doi.org/10.52202/077185-0020

REFERENCES

Belgasim, B., Aldali, Y., Abdunnabi, M. J. R., Hashem, G., & Hossin, K. (2018). The potential of concentrating solar power (CSP) for electricity generation in Libya. *Renewable and Sustainable Energy Reviews*, *90*, 1–15. https://doi.org/10.1016/J.RSER.2018.03.045

Bellos, E., Tzivanidis, C., & Antonopoulos, K. A. (2017). A detailed working fluid investigation for solar parabolic trough collectors. *Applied Thermal Engineering*, *114*, 374–386. https://doi.org/10.1016/J.APPLTHERMALENG.2016.11.201

Bellos, E., Tzivanidis, C., Antonopoulos, K. A., & Daniil, I. (2016). The use of gas working fluids in parabolic trough collectors – An energetic and exergetic analysis. *Applied Thermal Engineering*, *109*, 1–14. https://doi.org/10.1016/J.APPLTHERMALENG.2016.08.043

Boretti, A. (2023). Technology readiness level of photo-electro-chemical hydrogen production by parabolic dish solar concentrator. *International Journal of Hydrogen Energy*, *48*(90), 35005–35010. https://doi.org/10.1016/J.IJHYDENE.2023.05.350

David Sánchez Martínez, María Lourdes García-Rodríguez, Tomás Sánchez-Lencero, Antonio Muñoz-Blanco, Inés Méndez-Majuelo, Rafael González-Almenara, Blanca Petit, Blanca de Weert, & Juan Martín. (2019). *SOLMIDEFF (SOLar Micro gas turbine-driven Desalination for Environmental oFF-grid applications)*. Universidad de Sevilla. https://institucional.us.es/solmideff/

Escamilla, A., Sánchez, D., & García-Rodríguez, L. (2022). Assessment of power-to-power renewable energy storage based on the smart integration of hydrogen and micro gas turbine technologies. *International Journal of Hydrogen Energy*, *47*(40), 17505–17525. https://doi.org/10.1016/J.IJHYDENE.2022.03.238

García Ferrero, J. (2023). *Concentrating thermosolar systems for distributed energy generation, PhD thesis*. Universidad de Salamanca.

García Ferrero, J., Merchán, R. P., Santos, M. J., Medina, A., Calvo Hernández, A., Canhoto, P., & Giostri, A. (2023). Modeling a solar pressurized volumetric receiver integrated in a parabolic dish: Off-design heat transfers, temperatures, and efficiencies. *Energy Conversion and Management*, *293*, 117436. https://doi.org/10.1016/J.ENCONMAN.2023.117436

Gavagnin, G. (2018). *Techno-economic optimization of a solar thermal power generator based on parabolic dish and micro gas turbine.* University of Seville.

Giostri, A., & Macchi, E. (2016). An advanced solution to boost sun-to-electricity efficiency of parabolic dish. *Solar Energy*, *139*, 337–354. https://doi.org/10.1016/j.solener.2016.10.001

Ho, C. K., & Iverson, B. D. (2014). Review of high-temperature central receiver designs for concentrating solar power. *Renewable and Sustainable Energy Reviews*, *29*, 835–846. https://doi.org/10.1016/J.RSER.2013.08.099

International Renewable Energy Agency. (2023). *Renewable Power Generation Costs In 2022*. www.irena.org

Kalogirou, S. A. (2014). *Solar Energy Engineering* (Second Edition).

Lanchi, M., Montecchi, M., Crescenzi, T., Mele, D., Miliozzi, A., Russo, V., Mazzei, D., Misceo, M., Falchetta, M., & Mancini, R. (2015). Investigation into the Coupling of Micro Gas Turbines with CSP Technology: OMSoP Project. *Energy Procedia*, *69*, 1317–1326. https://doi.org/10.1016/J.EGYPRO.2015.03.146

Lemmon, E. W., Bell, I. H., Huber, M. L., & McLinden, M. O. (2013). NIST Standard Reference Database 23: Reference Fluid Thermodynamic and Transport Properties-REFPROP. Version 9.1; National Institute of Standards and Technology, Standard Reference Data Program. In *Version 10.0; National Institute of Standards and Technology:* https://www.nist.gov/publications/nist-standard-reference-database-23-reference-fluid-thermodynamic-and-transport

Merchán, R. P., Santos, M. J., Medina, A., & Calvo Hernández, A. (2022). High temperature central tower plants for concentrated solar power: 2021 overview. *Renewable and Sustainable Energy Reviews*. https://doi.org/10.1016/j.rser.2021.111828

https://doi.org/10.52202/077185-0020

Sathish, T., Suresh, P., Sharma, K., Saravanan, R., Saleel, C. A., Shaik, S., Khan, S. A., & Panchal, H. (2023). Zero emission /energy building heating through parabolic dish collector focused KNO3–NaNO3 and KNO3–NaNO3–NaNO2 PCM absorber: A case study. *Case Studies in Thermal Engineering*, *44*, 102854. https://doi.org/10.1016/J.CSITE.2023.102854

Schiel, W., & Keck, T. (2012). Parabolic dish concentrating solar power (CSP) systems. In K. Lovegrove & W. Stein (Eds.), *Concentrating Solar Power Technology* (Energy, Vol. 21, pp. 284–322). Woodhead Publishing . https://www.sku.ac.ir/Datafiles/BookLibrary/45/Concentrating%20solar%20power%20technology_%20Principles,%20developments%20and%20applications-Woodhead%20Publishing.pdf

Semprini, S., Sánchez, D., & De Pascale, A. (2016). Performance analysis of a micro gas turbine and solar dish integrated system under different solar-only and hybrid operating conditions. *Solar Energy*, *132*, 279–293. https://doi.org/10.1016/j.solener.2016.03.012

Senthil, R. (2021). Enhancement of productivity of parabolic dish solar cooker using integrated phase change material. *Materials Today: Proceedings*, *34*, 386–388. https://doi.org/10.1016/J.MATPR.2020.02.197

Wu, Z., Caliot, C., Flamant, G., & Wang, Z. (2011). Numerical simulation of convective heat transfer between air flow and ceramic foams to optimise volumetric solar air receiver performances. *International Journal of Heat and Mass Transfer*, *54*(7–8), 1527–1537. https://doi.org/10.1016/J.IJHEATMASSTRANSFER.2010.11.037

Zhu, J., Wang, K., Jiang, Z., Zhua, B., & Wu, H. (2020). Modeling of heat transfer for energy efficiency prediction of solar receivers. *Energy*, *190*, 116372. https://doi.org/10.1016/J.ENERGY.2019.116372

ACKNOWLEDGEMENT

R. P. Merchán acknowledges a postdoctoral contract co-financed by the European NextGenerationEU fund, Spanish “Plan de Recuperación, Transformación y Resiliencia” fund, Spanish Ministry of Universities, and Universidad de Salamanca (“Ayudas para la recualificación del sistema universitario español 2021-2022”). J. García-Ferrero also acknowledges a research contract (“Programa Investigo, Plan de Recuperación, Transformación y Resiliencia”) co-financed by the European NextGenerationEU, Junta de Castilla y León and Universidad de Salamanca.

https://doi.org/10.52202/077185-0020